2

SAND93-0091
Conf-931088--1

DISCLAIMER

ABSTRACT

When a hydrocarbon reservoir is subjected to a hydraulic fracture treatment, the cracking and slipping of the formation results in the emission of seismic energy. The objective of this study was to determine the advantages of using broadband (100 Hz to 1500 Hz) microseismic emissions to map a hydraulic fracture treatment. A hydraulic fracture experiment was performed in the Piceance Basin of Western Colorado to induce and record broadband microseismic events. The formation was subjected to four processes; break-down/ballout, step-rate test, KCL mini-fracture, and linear-gel mini-fracture. Broadband microseisms were successfully recorded by a novel three-component wall-locked seismic accelerometer package, placed in an observation well 211 ft (64 m) offset from the treatment well. During the two hours of formation treatment, more than 1200 significant microseismic events were observed. The occurrences of the events strongly correlated with the injection bore-hole pressures during the treatments. Using both hodogram analysis and time of arrival information, estimates of the origination point of the seismic events were computed. A map of the event locations yielded a fracture orientation estimate consistent with the known orientation of the stress field in the formation. This paper describes the technique for acquiring and analyzing broadband microseismic events and illustrates how the new broadband approach can enhance signal detectability and event location resolution.

INTRODUCTION

Some form of stimulation, usually hydraulic fracturing, is required for the economic production of gas from tight reservoirs. A long-sought objective has been the incorporation of hydraulic fracture models with real-time diagnostic measurements of the fracture process. One potential diagnostic technique involves the monitoring of induced seismic emissions (commonly referred to as acoustic emissions, microseismic events, or microseisms) to map the hydraulic fracture field [1]. The measurement methodology involves the placement of one or more seismic sensors in either the stimulation well or an adjacent monitoring well to determine the origin of the microseismic events. Typically, a wall-locking three-component geophone instrument is utilized to sample the vector wave-field produced by the microseisms. The data from the three geophones is then processed such that the particle motion polarization is used to infer the orientation of the fracture plane [2]. In order to utilize the polarization approach, however, the seismic receiver instrument must faithfully record the particle motion of the seismic wave-field that is incident on the borehole. The conventional wall-locking geophone instrument generally does not enable the accurate measurement of particle motion over a wide frequency range [3,4]. The limited frequency range results from both locking resonances in the clamp sensor module and from the high frequency limitations of conventional geophones. In order to overcome the limitations presented by the wall-locking geophone system, an alternative borehole seismic receiver was utilized to extend the useable frequency range out to 1500 Hz. The novel receiver utilizes a novel clamp mechanism which enables its resonant frequency to be above 2000 Hz. Additionally, solid-state accelerometers are used as the sensing device, thereby eliminating spurious modes, phase errors, and high frequency noise limitations. The resulting seismic receiver is potentially capable of accurate particle motion measurement to frequencies nearly an order of magnitude higher than previously reported. This suggests that much improved detection and location of microseismic events can be obtained to map a hydraulic fracture.

The remainder of this paper will focus on an experiment in which a broadband accelerometer-based seismic receiver was

References and illustrations at end of paper

870

used to measure microseisms generated by hydraulic fracture treatments. In particular, the experiment described herein was utilized to determine the potential of an existing Western Colorado site for future, more sophisticated fracture diagnostic tests that will be conducted by the Gas Research Institute and the U.S. Department of Energy. At issue were:

1. Would microseisms be generated in significant numbers during a hydraulic-fracture treatment so that mapping would be effective in delineating fracture geometry;

2. Were the microseisms adequately analyzable in terms of clear P- and S-wave arrivals and highly polarized P-waves so that distance and orientation could be resolved;

3. What were the effects of the layered medium that would need to be accounted for in a fully developed site (e.g., multi-station receivers, separation of the stations, information on the velocity structure, etc.);

4. What were the characteristics of the microseisms (e.g., frequency content) that would need to be considered in developing a diagnostic plan for the site, and;

5. What processing techniques would be required to fully extract the important information.

To address these issues, the following paragraphs will describe the characteristics of the observed microseisms, outline the methodology for analyzing such events, and will develop a strategy for mapping the induced fractures.

THEORY

Microseism Generation, Propagation, and Measurement

Acoustic emissions resulting from a hydraulic fracture are generally caused by shear failures induced by the open, pressurized fracture and the localized high pore pressure zone surrounding the fracture [1]. Since these acoustic emissions are not believed to be caused by tensile failure as the hydraulic fracture propagates through the reservoir, they should occur in a band near the hydraulic fracture face. In this paper, it will be assumed that the formation surrounding the fracture face exhibits a homogeneous and isotropic velocity structure. Thus, the generated wavefield consists of a direct shear wave (S-wave), as well as a direct compressional wave (P-wave) conversion at the shear-failure interface. Both the S-wave and P-wave propagate outwardly from the source mechanism location. As these wavelets propagate through the formation, they undergo attenuation, and also cause secondary events (such as reflections, refractions, and mode conversions at interface boundaries) to occur. At any position in the formation, the resulting seismic waveform is the superposition of the direct P- and S-wavelets with the secondary wavelets. Within most formations of interest, the first wavelet in the complex wavefield is the direct P-wave energy that has travelled in a quasi-straight line from the source mechanism to the observation location. In order for the direct P-wave to arrive first and along a straight path, the formation must be weakly layered and must not contain large seismic velocity contrasts. If these conditions are met (as can be assessed from sonic logs), then one can assume that the first arrival in the wavefield has a particle motion which is collinear with the straight-line path between the microseism origin and the observation point. This assumption will be used in the remainder of this paper.

The technique for measuring the complex seismic wavefield involves multi-component vibration sensors emplaced within a borehole. The introduction of the borehole will preserve the incident seismic wavefield if the casing is properly cemented to the formation and the diameter of the drilled-hole is significantly smaller than the wavelengths of the propagating waves. The measurement of the wavefield using vibration sensors is precise only if the sensors are completely coupled to the borehole over the frequency band of interest.

Microseism Analysis for 3-component System

Microseisms have value for hydraulic fracture mapping only if the spatial location of the source mechanism can be determined from the recorded seismic wavefield. When a single tri-axial receiver is used to measure the wave-field, the source-mechanism location can be estimated by using information contained in both the direct P-wave and direct S-wave arrivals. This single receiver approach determines the event distance from the separation in time between the P- and the S-wave and the event orientation from the polarization of the P-wave. Such an analysis procedure has been documented previously by Thorne and Morris [5], Sarda et al.,[6] and Stewart et al.[7].

The orientation of the signal was the simpler part of the analysis in this experiment. The polarization analysis was conducted by determining the arrival time of the direct P-wave (the first arrival) and comparing the amplitude of the signals from the two horizontal axes for about 1.5 waveform cycles. The amplitude comparison was done using hodogram plots, circular statistics [8], rms values, and linear least squares analysis, yielding an azimuth estimate for the event. Given the azimuth, the vector sum of the amplitude along this horizontal azimuth was computed, and a similar comparison between the vertical axis and the horizontal vector sum yielded an inclination estimate for the event. Circular statistics were then applied to arrive at standard deviations for both the azimuth and inclination estimates.

The scheme for determining the distance of the source location from the seismic receiver location involves the time-tagging of the direct P- and direct S-waves. Assuming an incident signal has identifiable P-and S-waves, the distance, d, to the source is given by

$$d = \frac{V_p V_s}{V_p - V_s} (t_p - t_s)$$

where V_p is the P-wave velocity, V_s is the S-wave velocity, t_p is the time of arrival of the P-wave, and t_s is the time of arrival of the S-wave. Accuracy of this estimate is dependent on knowledge of the sonic velocities and determination of the arrival times. In this application, P- and S-wave velocities were

obtained from a long-spaced sonic log, yielding values of 14,300 ft/sec (4359 m) and 9100 ft/sec (2774 m) respectively for the sandstone.

The P-wave arrival time was obtained by locating the position at which the microseism appeared to rise out of the background noise and back-stepping sample-by-sample as far as the signal remained polarized. This point was usually clearly identifiable. The S-wave arrival is more difficult to determine, since it resides in the coda of the P-wave and is obscured by reflections and refractions. Three characteristics were used to identify the s wave, although most signals did not exhibit all three. First, since the S-wave is expected to have significant energy, the largest amplitude portion of the event was considered as the most-likely candidate. Second, the S-wave should have a 90° shift in polarity from the P-wave, so polarization of the signal was checked throughout the event to determine where such a shift occurred. And finally, since the S-wave's center frequency is expected to be different from the P-wave (generally lower), frequency shifts were noted. It was generally possible to find points in the microseism where at least two of these three conditions could be met.

Error analyses of the distance estimate are problematic, since it is difficult to assign error bounds to the in-situ velocities and the arrival time estimates. P-wave arrival time estimates are relatively certain due to high signal-to-noise conditions, but S-wave arrivals are occasionally obscured by complexities of the microseismic signal.

A map of the events is obtained by plotting the distance and orientation from the receiver well for each of the points for which location data appear to be reliable. There is a 180° ambiguity in the orientation estimates, but since the receiver well is offset from the treatment well and the fracture is expected to be planar and to originate in the treatment well, the 180° ambiguity is easily remedied.

EXPERIMENT SITE DESCRIPTION

This hydraulic fracture experiment was conducted at the GRI/DOE-funded M-Site, located in the Piceance basin of western Colorado near the town of Rifle. This site is currently being developed into a test facility for hydraulic-fracture diagnostic and modeling research. Depths of the test zones are 4000-5000 ft (1219-1524 m). Previously, the Multiwell Experiment [9] and Slant-Hole Completion Test [10] had been conducted at this site at greater depths.

Two wells, designated MWX-2 and MWX-3, were available for these tests. As shown in Figure 1, MWX-3 was the treatment well and is located approximately 210 ft (64 m) north of MWX-2, the observation well. Based on previous site data, the treatment was expected to propagate in a N60°W to N70°W direction [11]. The sandstone interval chosen for this test is at a depth of 4900-4946 ft (1494-1508 m) in MWX-3, as shown in the gamma-ray logs in Figure 2. This interval is a fluvial sandstone of the Cretaceous Mesaverde group. It is non-productive in this area because of low permeabilities (<0.1 md, <0.0001 m^2) and high water saturations (70-80%). Stress contrasts between the sandstone and the abutting materials are relatively small [12], and considerable fracture height growth was expected. The perforations were located from 4900-4920 ft (1494-1500 m) and 4930-4946 ft (1503-1508 m) at 2 shots per foot (1 shot per 0.6 m).

DESCRIPTION OF EQUIPMENT

Need for Novel Seismic Receiver

In order to utilize the polarization approach for event mapping, the seismic receiver instrument must faithfully record the particle motion of the seismic wave-field that is incident on the borehole. The conventional wall-locking geophone instrument generally does not enable the accurate measurement of particle motion over a wide frequency range. Two instrument limitations can cause the wall-locked geophone to record inaccurate particle motions. The first limitation, known as locking resonance, results from inadequate coupling of the geophones to the borehole over a wide frequency band [4]. When the locking arm of the instrument extends to clamp the unit to the borehole, the geophones are coupled to the borehole only at relatively low frequencies. At some higher frequency, the motions of the clamping unit do not follow the motions of the borehole wall. In conventional VSP geophone receivers, the resonant frequency of the clamped receiver is typically in the 200 Hz to 400 Hz range. Therefore, conventional VSP instruments can only be used for accurate polarization measurements for seismic excitations below about 200 Hz. In order to extend the frequency range above this limit, one must either use a novel clamping package or cement the geophones directly into the formation.

The second limitation in using the polarization method is that the geophone itself often does not accurately measure particle motion over a wide frequency range. Conventional geophones exhibit spurious modes which are due to off-axis excitation of the geophone springs [13]. The spurious mode manifests itself as a resonance effect which occurs at a frequency which is approximately 25 times higher than the natural frequency of the geophone. For example, a 10 Hz geophone can exhibit spurious modes at and above 250 Hz, thus limiting its usefulness above 250 Hz. Additionally, the low frequency end of the geophone does not accurately measure particle motion due to phase shifts within the first few octaves above the natural frequency. Even if these inaccuracies in the sensor could be eliminated or corrected for, the geophone suffers from high-frequency self-noise [14] which reduces the potential signal-to-noise ratio above approximately 200 Hz.

Accelerometer-Based Seismic Receiver

The accelerometer-based Advanced Borehole Receiver, available from OYO Geospace Corp., Houston, Tx. [14] was utilized as the seismic receiver for these experiments. The receiver consists of two pressure housings fitted with standard Gearhart-Owens seven conductor cable-heads, one on either end of the clamping section. One housing contains the tri-axially arranged accelerometers. The orientation of the accelerometers are vertical, parallel to the clamp mechanism travel direction, and perpendicular to the clamp travel direction. The other housing

contains the electric gear-motor assembly. This gear-motor drives the rectangular piston perpendicular to the longitudinal axis of the tool through the use of a 1:1 right angle gearbox to clamp the tool into the borehole.

Finite element analysis of the tool was previously performed to assure the clamping mechanism would maintain the potential for a flat tool response out to 2.0 KHz. The analysis resulted in a clamping piston design with 1.5 inches of travel, and accommodation of adapters to allow for clamping into boreholes ranging from 4.25 inches to 9 inches in diameter. The clamp force to tool weight ratio developed by this design is a function of the gearset selected to mate with the electric motor, and can vary from 5:1 to 20:1.

The low-noise piezo-electric accelerometers utilized in the receiver offer significant advantages over conventional geophones. In particular, these accelerometers do not exhibit the spurious resonance problem common to geophones. Additionally, accelerometers are insensitive to their mounting orientation and therefore do not require the gimbal mounts often utilized in geophone-based sondes. Another difference, and perhaps most important, is that these custom-designed low-noise piezo-electric accelerometers are more sensitive than geophones at the higher seismic frequencies. The high-frequency sensitivity improvement is due to the fact that the electronic noise of the custom accelerometer is lower than the electronic noise of the best geophones at frequencies above approximately 150 Hz. To illustrate this point, Figure 3 displays the seismic noise level in deep wells as compared to the noise limits of both geophones and accelerometers (the 2300 Hz accelerometer is the unit used in these experiments). It is apparent from Figure 3 that the accelerometers can offer as much as a 10:1 improvement in signal detection (and hence signal-to-noise ratio) at 1000 Hz. This signal-to-noise improvement has been demonstrated with this accelerometer receiver in numerous wells throughout the U.S. The specifications for these unique borehole accelerometers were developed by Sandia and resulted in a custom sensor which is now available from Wilcoxon Research as model 731-20.

Data Acquisition

The standard Gearhart-Owens seven conductor interface on the receiver allowed each accelerometer to use one pair of conductors with the motor using the center conductor and armor for electrical connection. With ground established at the tool, the accelerometers electrically isolated, and the armor at ground potential, battery operated constant current power supplies uphole eliminated 60 Hz interference on the 12000 ft wireline. The power supplies provide 20 dB of uphole amplification in addition to the downhole preamplification of 30 dB.

The analog accelerometer signals from the uphole preamplifier were directly digitized for subsequent analysis. For the perforation orientation shots (described below), the signals were digitized by an EG&G 2420 seismograph at a sample rate of 4000 samples per second. For recording microseisms during the hydraulic fracture experiment, continuous digital recording of the data was required. The accelerometer signals were continuously digitized and stored on a Sony model PC208 8-channel Digital Audio Tape (DAT) recorder at a sample rate of 12000 samples per second per channel. The DAT equipment was particularly well suited for this application since the signals are sampled simultaneously on all channels with a dynamic range of 85 dB, with each standard DAT tape capable of recording continuously for 3 hours. The digital data from the DAT can either be directly downloaded into a Personal Computer for further analysis, or redigitized by another recorder (if higher sample rates were desired). The data presented in this paper were redigitized by an EG&G 2401 seismograph at a rate of 20000 samples per second and were directly analyzed on the PC. Analysis of the digital seismic data was performed on a Compaq/486 system running both MicroMax software and Sandia-developed microseismic analysis software.

EXPERIMENTAL PROCEDURES

The three-component accelerometer receiver was placed in well MWX-2 at a depth of 4881 ft (1489 m), which is located 211 ft (64 m) south of the treatment well, MWX-3. In order to assure good coupling of the receiver to the scaled steel-casing, the receiver was clamped with approximately 50 lbs (220 N) of force, then slowly dragged up the hole while increasing the clamp force to 150 lbs (670 N). This assured that the receiver was centered in the hole and that minimal scaling remained between the clamp arm and the casing. Once the receiver was locked in at 4881 ft (1489 m), its orientation was determined from the detonation of charges in MWX-3. Ten decoupled 3.5 gm perforation charges were detonated and the recorded seismic signals were utilized to determine the absolute orientation of the receiver. Passive seismic data were recorded continuously during all four injections described below.

Hydraulic-fracture treatments were conducted during the week of October 13, 1992 by a standard service company, and consisted of four injections including a breakdown/ballout and a step-rate test and two minifracs. The treatment well was configured with $2^{7}/_{8}$-in tubing in 7-in casing; bottom of the tubing was at 4879 ft (1487 m). During the breakdown, a ballout of the perforations was performed and the treatment was pumped down the tubing. Only surface pressure was available during this test. For the other three injections, a wireline-run, surface-readout, bottom-hole pressure gauge was located just inside the bottom of the tubing, and the treatment was pumped down the annulus. A bridge plug was located at 5540 ft (1689 m).

The observation well, also 7-in casing, was left open for the seismic receiver instrumentation. A bridge plug was set at 5528 ft (1685 m) to control open perforations below. Six sets of open perforations were above the treatment interval, but they did not produce any significant gas flow and no noticeable effects were found.

Important information on the four treatments are shown in Table 1. The step-rate test was conducted for closure stress information. The two minifracs were conducted with different fluids in order to observe the effect that viscosity would have on the treatments. Each injection was followed by a long shut-in

period, a blow-down of pressure, and some additional time for reservoir equilibration before the next test. Pressures and rates were recorded continuously so microseismic events could be correlated with treatment parameters. During the injections, several shut-ins and rate changes were performed in order to evaluate near wellbore effects. As will be seen later, these injection changes had a significant influence on the microseismicity. Measured net pressures for these treatments were approximately 600-800 psi (4.1-5.5 MPa).

RESULTS

Background Seismic Noise

Background noise levels recorded by the locked accelerometer receiver were extensively studied. The ambient background noise level was particularly low, even though the seismic monitoring well is situated near active producing gas wells. The nominal background noise was -150 dB relative to 1 g/$\sqrt{Hz}$ (1 g = 9.8 m/sec/sec) at frequencies between 70 Hz and 400 Hz, and decreased to -160 dB at and above 1000 Hz. The recorded noise floor is lower than the electronic noise floor obtainable with geophones. This low noise floor is an attribute of the extremely low electronic self-noise of the accelerometers, and enabled the detection of even the weakest broadband events. The rms background noise was primarily dominated by low frequency cultural phenomena and was typically 1 micro-g rms. During pumping of fluids into the treatment well, the background noise increased by approximately 12 dB throughout the frequency spectrum and resulted in a maximum rms noise of 4 micro-g. The increased noise during pumping was attributed to both flow noise from the fluid and low-level seismic activity due to fluid injection into the formation.

Orientation of Receiver from 3.5 gm Charge

The seismic energy released from the 3.5 gm charges in well MWX-3 were recorded by the seismic receiver situated in well MWX-2. This cross-well geometry enabled the absolute azimuth of the receiver to be determined relative to the known MWX-2/MWX-3 azimuth. As an example of a typical cross-well recording, Figure 4 displays the three accelerometer signals from the clamped seismic receiver. The recorded signals have a broad energy spectrum from 100 Hz to 1500 Hz and exhibit a signal-to-noise ratio in excess of 70 dB. The first arrival of the P-wave is clear, and the primary energy is arriving on the y-channel. Figure 5 shows an overlay of the two horizontal channels and the corresponding polarization plot, indicating the relative orientations in the horizontal and vertical planes. The polarization plot clearly shows that the receiver y-axis is pointing almost directly north, which is the orientation of MWX-3 relative to MWX-2.

Number of Microseisms Recorded

In order to determine the number of events recorded during the injections, the accelerometer signals were peak-detected at a threshold of 40 micro-g, and the number of detected events were counted. Since the maximum background noise was 4 micro-g rms, the peak-detector counted the number of events with signal-to-noise ratios of at least 10:1. In all, more than 1200 microseismic events were counted in this manner during the two hours of injections and shut-ins. Figures 6,7,8, and 9 show the number of significant events occurring during the breakdown/ballout, step rate test, KCL mini-frac, and gel-mini-frac respectively. Each bar interval displayed in the histograms of Figures 6-9 represents 30 seconds of analysis time. Also plotted in Figures 6-9 are the corresponding treatment-well pressures occurring during the treatments. It is evident that the seismic activity, i.e. the generation of fracture-induced microseisms, correlates with the resulting treatment-well pressures.

After the breakdown, as indicated in Figure 6, there are approximately 20 microseisms per 30 second interval during the pumping. After the shut-in, the number of generated microseisms quickly diminished. Note that the step-rate test, as indicated by Figure 7, resulted in fewer events than the breakdown/ballout test, and that most of the observed signals occurred during high flow-rate periods. Comparing figures 8 and 9, the gel minifrac resulted in nearly twice as many seismic events as the KCL mini-frac. This result is consistent since roughly twice the volume of fluid was injected during the gel mini-frac. The important point to note is that a large number of microseisms were generated by hydraulic fractures of even modest size (e.g. the breakdown and step-rate tests).

Spectral Content of Microseisms

In order to determine the useful bandwidth of the microseismic events, Fourier spectra were computed from the raw accelerometer signals. Results of spectral averaging of 256 detected events (those with peak amplitude greater than 40 micro-g) during the gel mini-frac are displayed in Figure 10. The spectral content is provided for each of the three accelerometers in the downhole receiver, and for reference, the measured seismic noise floor is plotted. It is clear from Figure 10 that excellent signal-to-noise is available throughout the measurement frequency band of 100 Hz to 1500 Hz. At frequencies below 100 Hz, ambient background noise becomes comparable to the microseismic signal strength. Above 1500 Hz, resonances in the clamped accelerometer package and the accelerometers themselves begin to affect the coherency of the three components. Noting that the spectral content of all three accelerometer signals is comparable in the 100 Hz to 1500 Hz range, we conclude that this entire bandwidth is free of resonance effects and can be used in the polarization analysis.

Example Microseismic Event

A plot of a typical microseismic event is depicted in Figure 11. Both the P-wave and S-wave arrivals are clearly delineated in the event. The frequency spectra for both the microseismic event and the pre-event noise are plotted in Figure 12. Note that for this event, significant energy occurs above 250 Hz, confirming the need for broadband measurements.

ANALYSIS AND INTERPRETATION OF DATA

The objective of this study was to determine the advantages of using broadband microseismic emissions to estimate the hydrau-

lic fracture geometry. To illustrate how the theory described above is applied, consider the example microseismic event of Figure 11. The three accelerometer signals of Figure 11 are over-plotted in Figure 13a. The overlay indicates that during the P-wave arrival, all three accelerometers are in-phase, i.e. that the particle motion is essentially linearly polarized. The majority of microseisms recorded during this experiment exhibit this feature, implying that the polarization approach is appropriate. Figures 13b and 13c plot the polarization for the example event. The least-squares linear fit of the polarization plot is used to estimate the orientation of the source-mechanism relative to the receiver. By measuring the time delay between the P- and S- arrivals, and using the known seismic velocities in the formation, a range estimate of the event origin may also be formulated.

Since the objective of this test was to determine the characteristics of the microseismic emissions (for planning the experimental site), there was no attempt to obtain a detailed fracture map. Instead, 67 events were arbitrarily selected from the four injections and were analyzed for polarization, P-S separation, spectral characteristics, and other useful information. Of these 67 signals, 47 were found to be suitable for event-location analysis and were analyzed in the fashion described above. The group of 47 events consisted of both strong and weak events from all four well-treatments. As expected, the stronger events yielded lower error bounds due to higher signal-to-noise ratios. A plan-view map of the event location estimates using the selected 47 events is provided in Figure 14 . From Figure 14, the apparent azimuth of the hydraulic fractures is estimated at N65°E. This estimated fracture azimuth is consistent with the known stress field at this site previously determined from extensive hydraulic fracture experiments and core analysis. The half-length of the east wing appears to be at least 200 ft (61 m) to 300 ft (92 m). While the east wing is fairly well described, the west wing has relatively few data points, resulting from the larger microseismic propagation distance and possibly due to increased attenuation through the stress field. It is believed that the hydraulic fracture could be more completely described if additional microseisms were analyzed, but such an additional effort was beyond the scope of this experiment.

A side view of the estimated microseismic locations is shown in Figure 15. The estimates are all situated within a 350 ft (107 m) vertical band, with most of the estimates within a 200 ft (61 m) vertical band centered around the treatment depth. In general, the inclination estimates exhibit larger errors than the corresponding azimuth estimates. The larger errors are due in part to the layering of the formation and the resulting complex vertical wavefield. The vertical errors could be reduced substantially if multiple seismic receivers were placed in the observation well, and inclination and range were determined from first-arrival move-out.

RECOMMENDATIONS FOR SEISMIC MONITORING

In order to obtain optimal data, it is advantageous to use a seismic receiver that can detect the broadband emissions without the distortions caused by tool resonances. Normal wall-locking tools, such as those used for VSP surveys, are not capable of faithfully recording the particle motion over a wide frequency range. Advanced tools, using novel clamp designs and modal analysis to eliminate unwanted resonances, can provide the necessary detection capabilities. It is also important to take special precautions to assure that the receiver is adequately coupled to the borehole, irrespective of casing conditions. Special clamp procedures should be developed and tested.

Advanced accelerometer technology provides significant enhancements over geophones for detection of broadband emissions. Accelerometers should be considered for all microseismic mapping experiments where high frequency data are considered important. Additionally, due to the different types and strengths of microseismic signals, it is imperative to record continuously on wide-band-width, wide-dynamic-range recorders.

While polarization and P-S separation techniques can provide estimates of the locations event origin, difficulties in determining S-wave arrival points and vertical-plane polarization (inclination) make single station receiver technology less accurate in layered media. Future testing should be conducted with multi-station receivers. Additionally, accurate determination of the absolute orientation of the receiver(s) is imperative. While cross-well shooting can be used to determine a reasonably accurate tool orientation, a gyro or other means should be considered for an accurate, ground-truth orientation of the receiver(s).

Microseismic fracture mapping will only become a viable technology if techniques are developed to automate the processing as much as possible. Only a small fraction of the detectable microseisms can be processed individually by an analyst, at considerable time and effort. Such desirable processing capabilities include a real-time event detector, event-location processing, spectral analysis, event activity histograms, and classification of signal types.

CONCLUSIONS

Significant microseismic activity was recorded in an offset monitoring well during a hydraulic fracture experiment in the Piceance Basin of Western Colorado. The microseisms were acquired with a novel three-component wall-locked seismic accelerometer package, which enhanced detection of the microseismic events. During two hours of formation treatment, more than 1200 microseisms with signal-to-noise ratios in excess of 20 dB were observed. Microseismic event activity was directly correlated with the induced borehole pressures in the treatment well. The observed microseisms had a nominally flat frequency spectrum from 100 Hz to 1500 Hz and lacked the spurious tool-resonance effects evident in previous attempts to measure microseisms. The recorded microseisms exhibited discernable P- and S- wave arrivals, and good coherency was obtained from all three components of the P-wave arrival. Using polarization analysis and P-to-S wave travel time differences, estimates of the microseismic event location were obtained. Using location estimates from a limited number of microseismic events, both plan-view and side-view maps of the fracture experiment were generated. The plan-view map of the estimated hydraulic fractures correlates with the known stress

field in the formation. The side-view map provides an indication that the hydraulic fracture height was approximately 200 ft (61 m). The accuracy of the hydraulic fracture maps can be improved by utilizing a larger set of microseisms and/or incorporating simultaneous measurements from multiple borehole seismic receivers.

ACKNOWLEDGEMENTS

This project was funded by the Gas Research Institute under contract number 5089-211-2059, managed by Steve Wolhart. The authors would like to thank Steve for his help and acknowledge the joint participation by the CER Corporation. In particular, we appreciate the able field support provided by Rich Peterson, Paul Branagan, Mike Middlebrook, and Roy Wilmer of CER Corporation.

REFERENCES

[1] Dobecki, T.L., "Hydraulic Fracture Orientation Using Passive Borehole Seismics," SPE 12110, 58th SPE Annual Technical Conference, San Francisco, CA, October 5-8, 1983.

[2] Sorrells, G.G., and Mulcahy, C.C., "Advances in the Microseism Method of Hydraulic Fracture Azimuth Estimation," SPE 15216, Proceedings, SPE Unconventional Gas Technology Symposium, Louisville, KY, pp. 109-120, May 18-21, 1986.

[3] Galperin, E.I., *Vertical Seismic Profiling and its Exploration Potential*, D. Reidel Publ. Co., Boston, MA, pp. 25-26, 1985.

[4] Gaiser, J.E., Terrance, J.F., Petermann, S.G., and Karner, G.M., "Vertical Seismic Profile Sonde Coupling," *Geophysics*, Volume 53, Pages 206-214, Feb., 1988.

[5] Thorne, B.J. and Morris, H.E., "Advances in Borehole Seismic Fracture Diagnostics, "SPE 16405, Proc. Symposium on Low Permeability Reservoirs, Denver, Co., pp. 165-172, May 18-19, 1987.

[6] Sarda, J-P., Perreau, P.J. and Deflandre, J-P., "Acoustic Emission Interpretation for Estimating Hydraulic Fracture Extent, SPE 17723, Proc. Gas Technology Symposium, Dallas, TX, pp. 183-191, June 13-15, 1988.

[7] Stewart, L., Cassell, B.R. and Bol, G.M., "Acoustic Emission Monitoring During Hydraulic Fracturing," *SPE Formation Evaluation*, Vol. 7, pp. 139-144, June 1992.

[8] Engi, D., "A Spherical Stochastic Methodology for Microseismic Event Location," *Computers and Geosciences*, Vol. 15, No. 7, pp. 1037-1052, 1989.

[9] Northrop, D.A. and Frohne, K-H., "The Multiwell Experiment - A Field Laboratory in Tight Gas Sandstone Reservoirs," *JPT*, Vol. 42, pp. 772-779, June 1990.

[10] Myal, F.R. and Frohne, K-H., "Slant-Hole Completion Test in the Piceance Basin, Colorado," SPE 21866, Proc. Rocky Mt. Regional/Low Permeability Reservoirs Symposium, Denver, CO, pp. 611-622, April 15-17, 1991

[11] Warpinski, N.R. and Teufel, L.W., "In Situ Stresses in Low-Permeability Nonmarine Rocks," *JPT*, Vol. 41, No. 4, pp. 405-414, April 1989.

[12] Middlebrook, M., Peterson, R., Warpinski, N.R., Engler, B., Sleefe, G., Cleary, M, Wright, T. and Branagan, P., "Multi-Site Project Seismic Verification Experiment and Assessment of Site Suitability," GRI-93/0050, GRI Topical Report, February 1993.

[13] Stanley, P.J., "The geophone and front-end fidelity," *First Break*, Vol. 4, No. 12, pp. 11-14, 1986.

[14] Sleefe, G.E. and Engler, B.P., "Experimental Study of an Advanced Three-Component Borehole Seismic Receiver," Proceedings, 61st Annual SEG Meeting, Houston, TX, pp. 30-33, 1991.

Table 1 Injection data

TEST	DATE	VOLUME	RATE	FLUID
BREAKDOWN	10/14/92	70 bbl	8 bpm MAX	40# X-LINK GEL
STEP-RATE	10/14/92	100 bbl	20 bpm MAX	KCl
KCl MINIFRAC	10/14/92	304 bbl	30 bpm MAX	KCl
GEL MINIFRAC	10/15/92	634 bbl	25 bpm MAX	40# LINEAR GEL

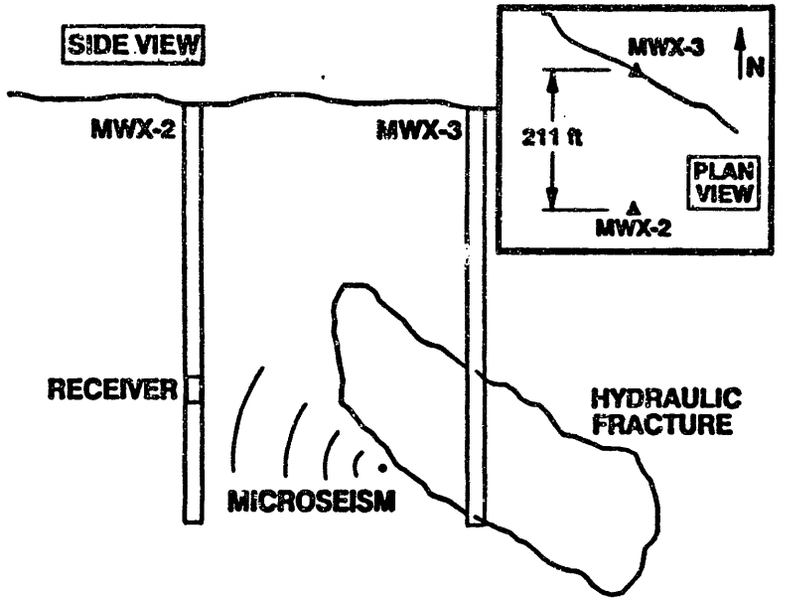

FIGURE 1 - SITE SCHEMATIC AND PLAN VIEW (insert)

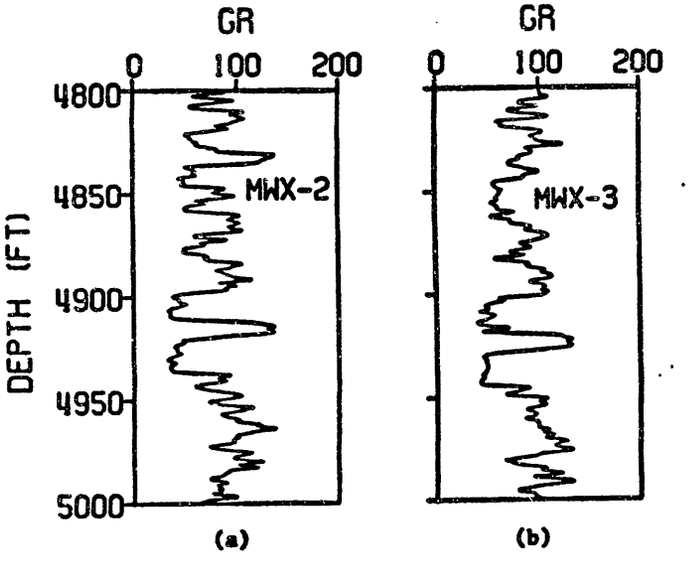

FIGURE 2 - GAMMA RAY LOGS FROM
a) well MWX-2, and b) well MWX-3

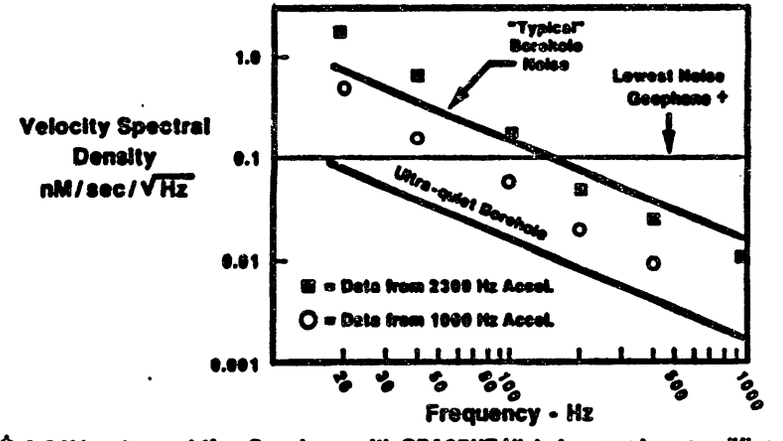

+ 0.5 V/cm/sec., 1 KΩ Geophone with OPA37HT High-temperature amplifier

FIGURE 3 -NOISE LIMITS OF BOREHOLE SEISMIC SENSORS

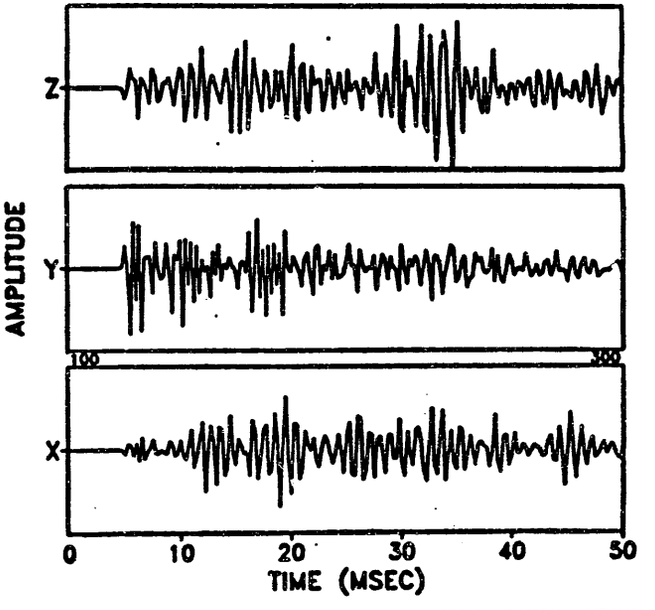

FIGURE 4 - THREE-COMPONENT ACCELEROMETER RECORDING
IN MWX-2 FROM 3.5gm CHARGE IN MWX-3

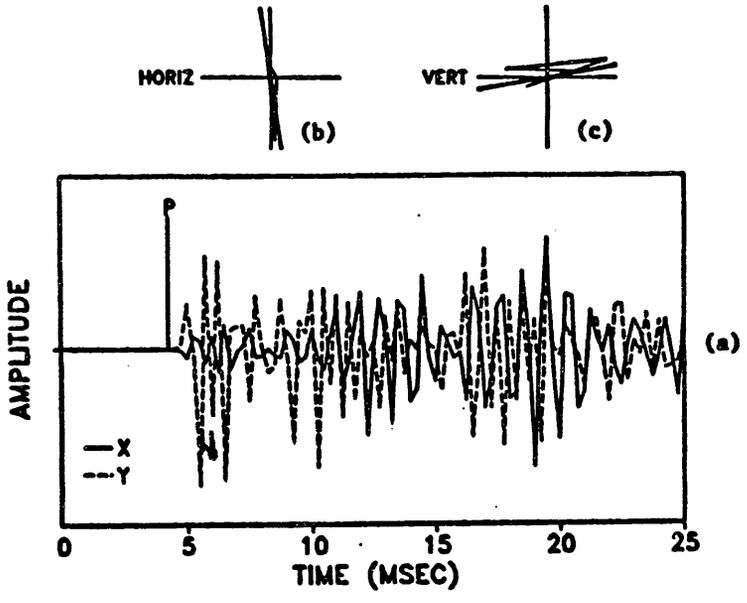

FIGURE 5 - a) OVERPLOT OF HORIZONTAL COMPONENTS OF FIG. 4,
b) HORIZONTAL HODOGRAM,
c) VERTICAL HODOGRAM

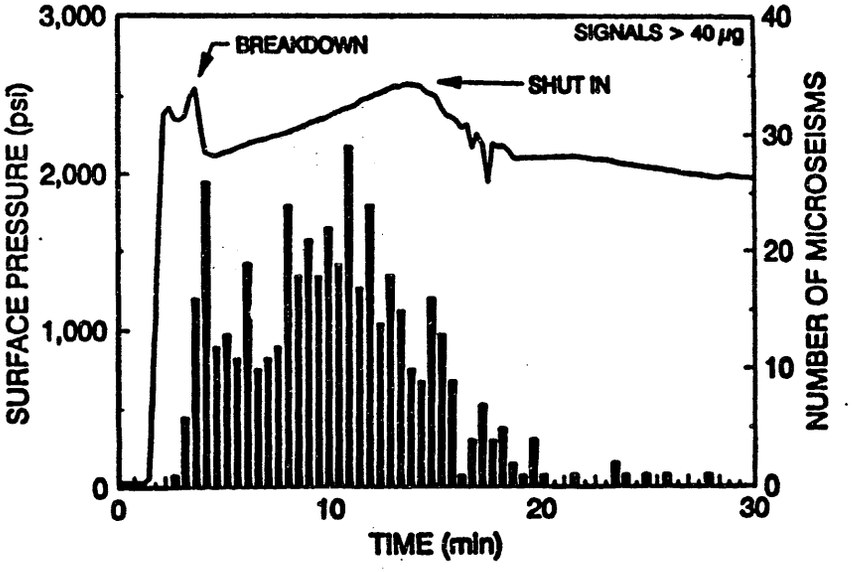

FIGURE 6 -MICRO-SEISMIC ACTIVITY DURING BREAKDOWN/BALL OUT AND CORRESPONDING TREATMENT PRESSURES

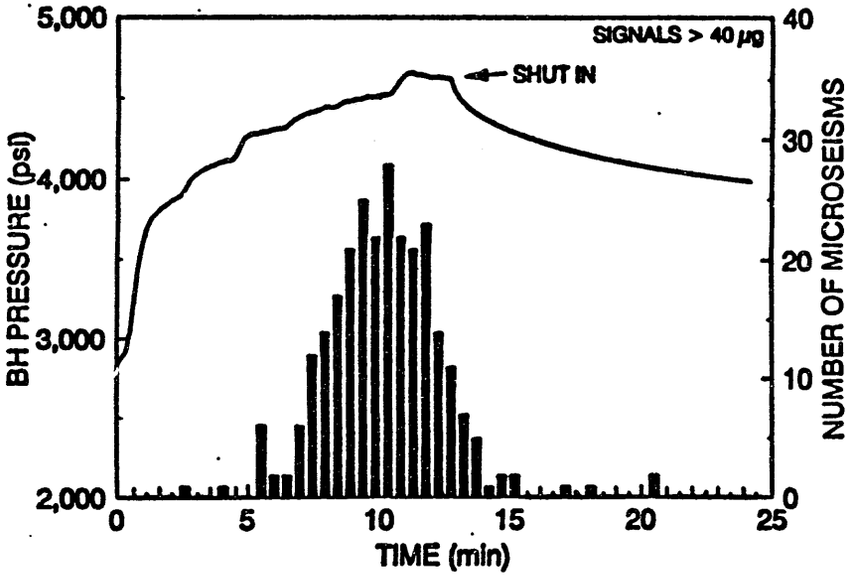

FIGURE 7 - MICRO-SEISMIC ACTIVITY DURING STEP-RATE TEST AND CORRESPONDING TREATMENT PRESSURES

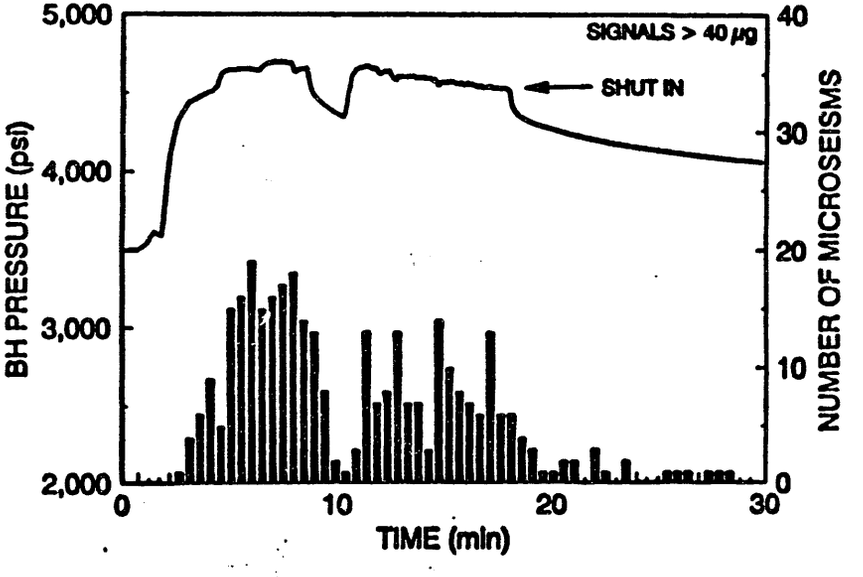

FIGURE 8 - MICRO-SEISMIC ACTIVITY DURING KCL MINIFRAC AND CORRESPONDING TREATMENT PRESSURES

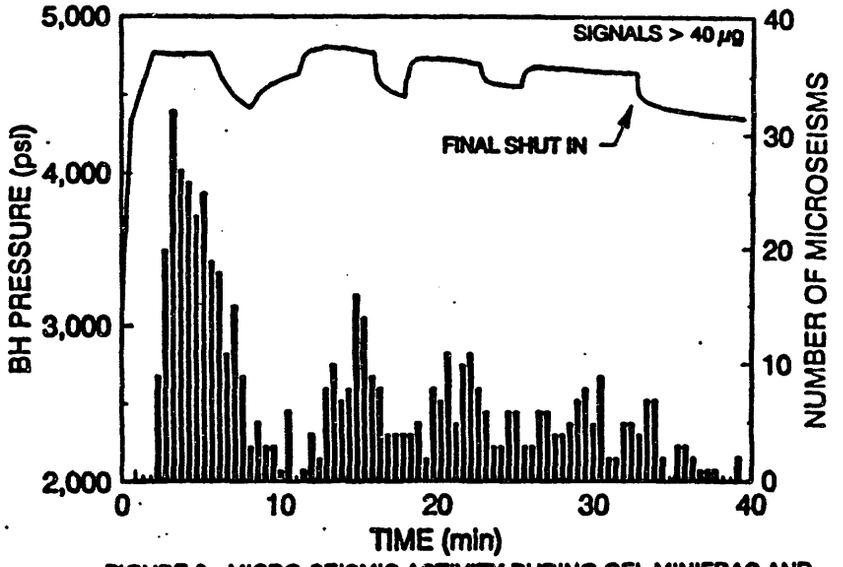

FIGURE 9 - MICRO-SEISMIC ACTIVITY DURING GEL MINIFRAC AND CORRESPONDING TREATMENT PRESSURES

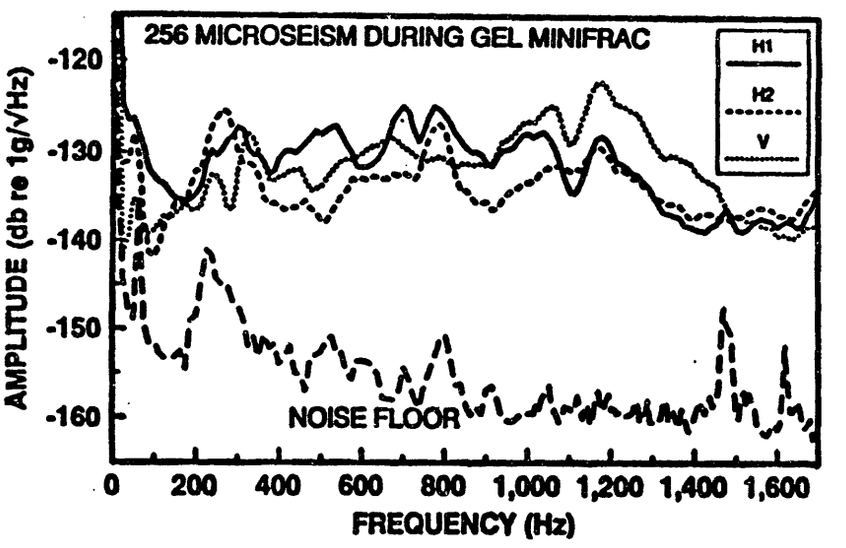

FIGURE 10 - MICRO-SEISMIC FREQUENCY SPECTRA FROM GEL MINIFRAC

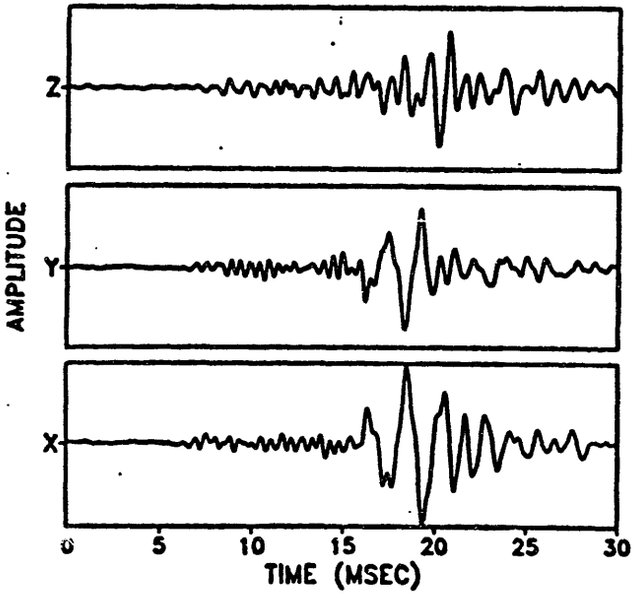

FIGURE 11 - TYPICAL MICRO-SEISMIC EVENT RESULTING FROM HYDRAULIC FRACTURE TREATMENT

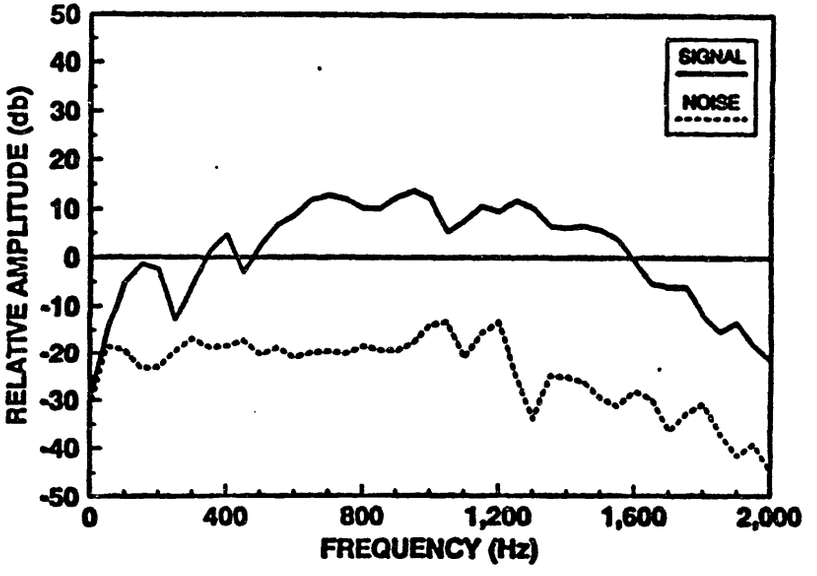

FIGURE 12 - VERTICAL COMPONENT SPECTRA FOR EVENT AND PRE-EVENT NOISE

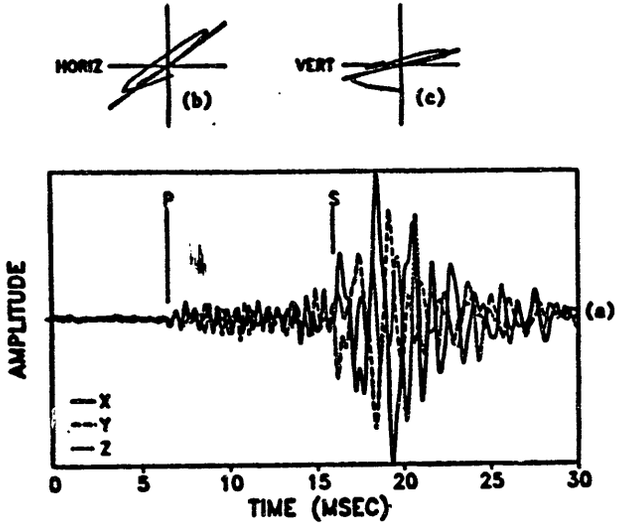

FIGURE 13 - a) OVER-PLOT OF MICRO-SEISMIC EVENT,
b) HORIZONTAL HODOGRAM,
c) VERTICAL HODOGRAM

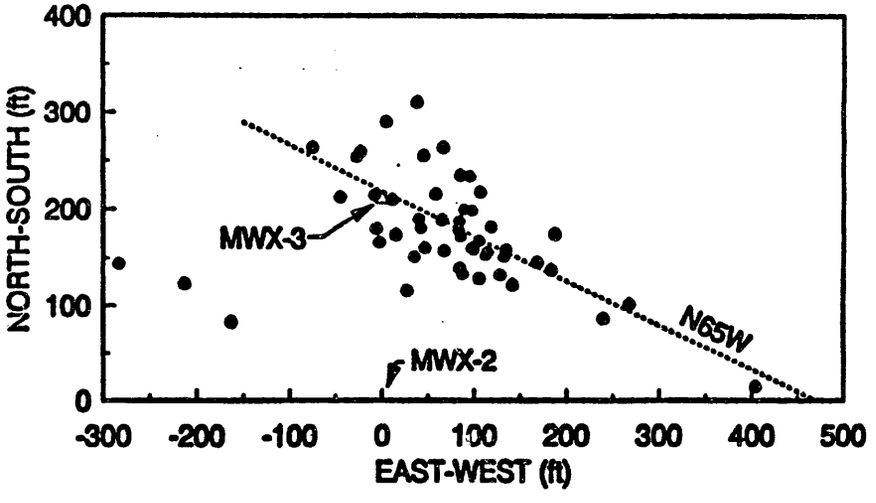

FIGURE 14 - PLAN VIEW OF MICRO-SEISM EVENT LOCATIONS

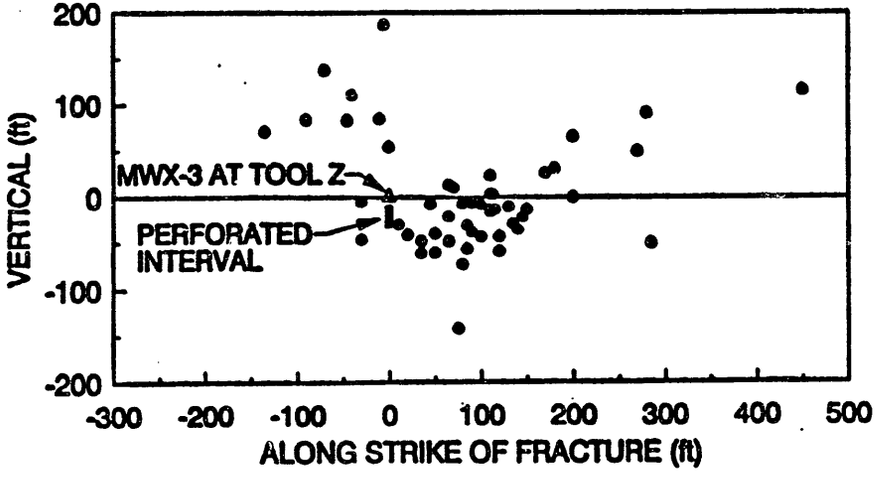

FIGURE 15 - SIDE VIEW OF MICRO-SEISM EVENT LOCATIONS

END

DATE
FILMED
11/5/93